ISSN 1975-8359(Print) / ISSN 2287-4364(Online)
The Transactions of the Korean Institute of Electrical Engineers Vol. 61, No. 12, pp. 1813~1819, 2012
http://dx.doi.org/10.5370/KIEE.2012.61.12.1813

전기강판의 벡터 자기특성을 고려한 전기기기의 손실특성 해석

Iron Loss Analysis of Electric Machine Considering Vector Magnetic Properties of Electrical Steel Sheet

윤 희 성* · 고 창 섭†
(Heesung Yoon · Chang Seop Koh)

Abstract - This paper presents vector magnetic properties of an electrical steel sheet (ESS) employed for electric machine and iron loss analysis considering the vector magnetic properties of the ESS. The vector magnetic properties of the ESS are measured by using a two-dimensional single sheet tester and modeled by an E&S vector hysteresis model to be applied to finite element method. The finite element analysis considering the vector magnetic properties is applied to iron loss analysis of a three-phase induction motor model, and the influences of the vector magnetic properties on the iron loss distribution are verified by comparing with numerical results from a typical B-H curve model.

Key Words : Iron loss, Electrical steel sheet, Electric machine, Vector magnetic properties

1. Introduction

Magnetic field and iron loss distributions in electric machines are strongly influenced by the magnetic properties of electrical steel sheet (ESS) employed. With the development of a two-dimensional (2D) single sheet tester (SST), it has been proven that the electrical steel sheet has complicated vector magnetic properties, which have spatial phase difference, between magnetic flux density (B) and magnetic field intensity (H) under alternating and rotating magnetic fields [1], [2].

Conventionally, the vector magnetic properties of the ESS have not been considered for magnetic field and iron loss analyses for the electric machines, and the magnetic properties of the ESS have been assumed simply as the scalar magnetic properties [3]. The assumption may lead to inaccurate analysis for the magnetic field and iron loss distributions of the electric machines. The vector magnetic properties of the ESS should, therefore, be considered in finite element analysis (FEA) for more precise analysis of the electric machines.

In this paper, the vector magnetic properties of the non-oriented ESS are presented, and their influences on the magnetic field and iron loss distributions of a three-phase induction motor model are investigated. The vector magnetic properties are measured by using 2D SST, and modeled via an E&S vector hysteresis model to be applied to FEA. Through comparisons with the analyzed results by a typical B-H curve model, the influences of the vector magnetic properties on the three-phase induction motor model are verified.

* College of Electrical and Computer Engineering, Chungbuk National University
† Corresponding Author : College of Electrical and Computer Engineering, Chungbuk National University
E-mail : kohcs@chungbuk.ac.kr
Received : July 2, 2012; Accepted : November 15, 2012

2. Vector Magnetic Properties of Non-Oriented Electrical Steel Sheet

2.1 Measurement System

Fig. 1 shows a vector magnetic measurement apparatus referred as a 2D SST. In order to generate magnetic flux along the rolling direction (RD) and transverse direction (TD) with respect to a specimen, the exciting windings are positioned to yoke poles lain on RD and TD. The specimen is located at the center of yoke poles, and two B-coils consisted of one turn of 0.08(mm) diameter are inserted to the center of the specimen to measure B-waveforms. The H-coils consisted of 40 turns of 0.05(mm) diameter are mounted at the bottom of the specimen to measure H-waveforms.

In order to obtain sinusoidal alternating and rotating magnetic fields, as defined in Fig. 2, at the center of the specimen, the exciting voltage-waveforms are controlled iteratively by comparing the desired B-waveforms with the measured ones from B-coils [4]. When the measured B-waveforms are coincided with desired ones via the waveform control function, the H-waveforms corresponding to the measured B-waveforms are obtained from H-coils [4].

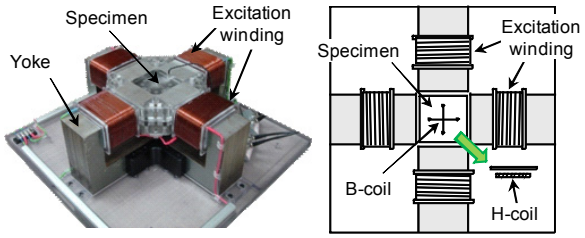

(a) two-dimensional single sheet tester

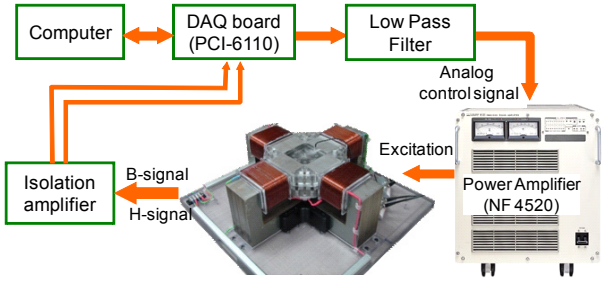

(b) measurement system

Fig. 1 Configuration of a two-dimensional single sheet tester.

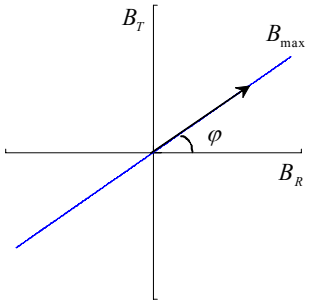

(a) alternating magnetic field

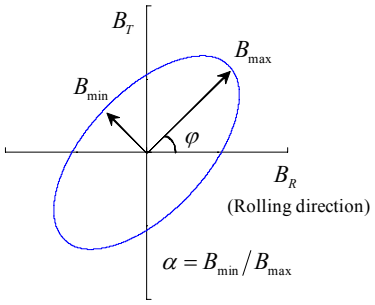

(b) rotating magnetic field

Fig. 2 Definition of a *B*-waveform.

2.2 Measured Results

Fig. 3 shows the measured *H*-waveforms, for the non-oriented ESS 50PN600, under pure rotating magnetic flux densities. It is observed that the magnitudes of *H* are changed with the rotation of *B* even though magnitudes of *B* keep a constant, and the reluctivity in TD is relatively larger than that in RD. This phenomenon results from the anisotropic property of the non-oriented ESS. In Fig. 3(b), it is found that there are phase differences between *B* and *H*, and the phase differences fluctuate by the influences of the vector magnetic properties of the ESS.

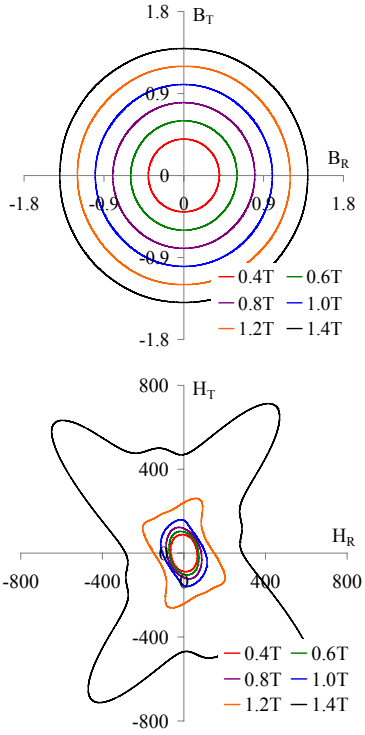

(a) measured *B*- and *H*-waveforms

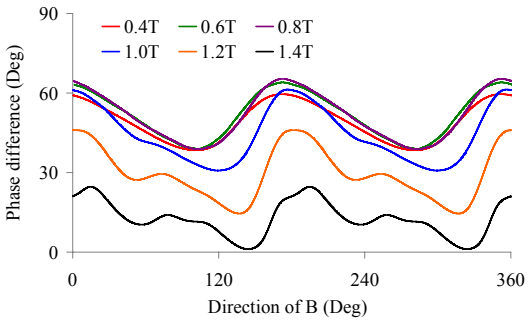

(b) phase difference between *B* and *H*

Fig. 3 Measured *H*-waveforms under pure rotating magnetic flux densities with variations of B_{max}.

Fig. 4 shows the measured results under the elliptically rotating magnetic flux densities when B_{max}=1.4(T) and a =0.5. Since the non-oriented ESS does not have the ideal isotropic property, the shapes of *H*-waveforms are changed according to the inclination angles of *B*-waveforms even though the shapes of *B*-waveforms are same. It is interesting that the maximum magnitude of *H*-waveform appears at the inclination angle of 60°, and

it means that the non-oriented ESS has the smallest permeability around not 90° (=TD) but 60°.

Fig. 5 compares the measured iron losses with variations of $B_{\max}$ and a when φ=0°. It is found that the iron loss for the rotating magnetic field is larger than that for the alternating one. This deviation of the iron loss between the alternating and rotating magnetic fields comes from the vector magnetic properties of the ESS, therefore, the vector hysteresis properties should be considered in the precise local iron loss estimation of the electric machine.

3. Finite Element Method Combined with E&S Vector Hysteresis Model

3.1 E&S Vector Hysteresis Model

In the E&S vector hysteresis model which includes the classical eddy current field, the relationship between magnetic flux density and magnetic field intensity in a electrical steel sheet is defined as follows [5], [6]:

$$\begin{Bmatrix} H_R \\ H_T \end{Bmatrix} = \begin{bmatrix} \nu_R & 0 \\ 0 & \nu_T \end{bmatrix} \begin{Bmatrix} B_R \\ B_T \end{Bmatrix} + \begin{bmatrix} h_R & 0 \\ 0 & h_T \end{bmatrix} \begin{Bmatrix} \partial B_{R1}/\partial\tau \\ \partial B_{T1}/\partial\tau \end{Bmatrix} + \frac{\sigma\omega d^2}{12} \begin{Bmatrix} \partial B_R/\partial\tau \\ \partial B_T/\partial\tau \end{Bmatrix} \quad (1)$$

where the subscripts R and T denote the RD and TD of the electrical steel sheet, respectively, τ stands for $\omega t \in [0, 2\pi]$ with ω as the angular frequency of the fundamental component of a B-waveform, ν and h are the magnetic reluctivity and hysteresis coefficients, respectively, B_1 is the fundamental component of a B-waveform, σ and d are the conductivity and thickness of the electrical steel sheet, respectively.

In order to calculate the magnetic reluctivity and hysteresis coefficients, databases are first constructed from various elliptic B-waveforms defined in Fig. 2 and their corresponding H-waveforms measured by using the 2D SST [5], [6]. For an arbitrary B-waveform, the corresponding H-waveform can be directly predicted from (1) with the coefficients interpolated from the databases via $(B_{\max}, \varphi, \alpha)$ of the B-waveform [5], [6].

3.2 Implementation to Finite Element Method

In order to apply the E&S vector hysteresis model to the finite element method (FEM), a governing equation is derived from Maxwell's equation as follows [6]:

$$\nabla\times[\nu]\nabla\times\vec{A} = \vec{J_0} - \nabla\times\left([h]\frac{\partial\vec{B_1}}{\partial\tau} + \frac{\sigma\omega d^2}{12}\frac{\partial\vec{B_{old}}}{\partial\tau}\right) \quad (2)$$

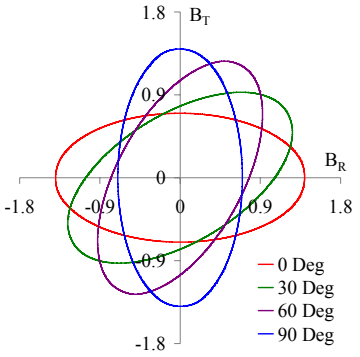

(a) measured B-waveforms

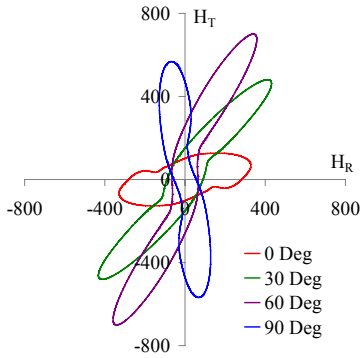

(b) measured H-waveforms

Fig. 4 Measured H-waveforms under elliptically rotating magnetic flux densities when $B_{\max}$=1.4(T) and a =0.5.

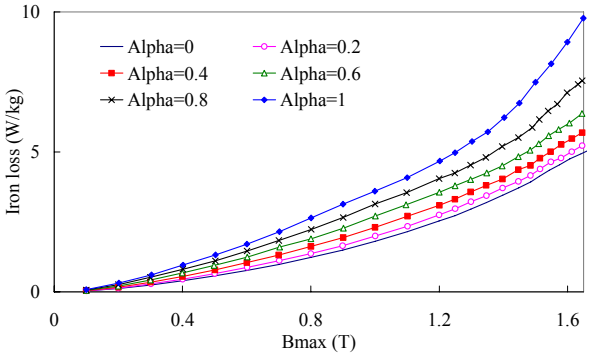

Fig. 5 Comparison of measured iron losses according to variations of $B_{\max}$ and a when φ=0.

where $\vec{A}$ and $\vec{J_0}$ are vector magnetic potential and applied current density, respectively, $\vec{B_{old}}$ is the B-waveform obtained in the previous iteration.

In the analysis, the external circuit equation is combined with (2) to give a time variant solution.

Since the magnetic reluctivity and hysteresis coefficients in (2) are expressed through $(B_{\max}, \varphi, \alpha)$ of a B-waveform, equation (2) together with the circuit equation is solved iteratively using a relaxation method as follows:

Step 1 Analyze the problem for one period by using typical FEM with the B-H curve model.

Step 2 For all elements, calculate $(B_{\max}, \varphi, \alpha)$ from the B-waveform.

Step 3 Calculate the magnetic reluctivity and hysteresis coefficients v and h from the databases, and analyze the problem for one period.

Step 4 Check the convergence of $(B_{\max}, \varphi, \alpha)$ for all elements.

Step 5 If converged, stop. Otherwise go to *Step* 6.

Step 6 Update $(B_{\max}, \varphi, \alpha)$ using relaxation method for all elements, and go to *Step* 3.

4. Iron Loss Analysis of Three-Phase Induction Motor Model

In order to emphasize the influences of the vector magnetic properties on the electrical machines, the numerical results by the E&S vector hysteresis model are compared with those by the typical B-H curve model which is one of the modeling methods describing the scalar magnetic property.

Fig. 6 and Table 1 show the specifications of a two-pole three-phase induction motor model of which applied voltage and frequency are 110(V) and 60(Hz), respectively. The motor model is made of the non-oriented silicon steel sheet 50PN600, and is assembled so that RD of the stator and rotor may coincide exactly with the x-axis. The rotor of the motor model does not have any conducting bars and is not rotated to make the experimental measurement easily.

In order to experimentally measure the magnetic flux linkages of each stator tooth and to see their differences according to their location, one-turn sensing coil is installed at each tooth as shown in Fig. 6(b).

Fig. 7 compares the calculated and measured maximum magnetic flux linkages $(\Phi_{\max})$ and their corresponding magneto-motive forces (*mmf*) for each stator tooth. It can be seen that the induction motor model has uneven *mmf* distribution due to its short winding pitch. Investigating the maximum magnetic flux linkages for the teeth having the same *mmf*, for example teeth (3, 9), it is found that the experimental measurement and E&S model give more flux linkages to tooth 3, which locates along the RD, than the tooth 9, while the B-H curve model gives almost same flux linkages for all teeth. This phenomenon, as reported in [7], comes from the anisotropic magnetic properties of the non-oriented ESS, and the E&S model takes the magnetic properties of the ESS into account properly while the B-H curve model not. The discrepancies between the measured and calculated flux linkages from the E&S model are considered to result from the skew effect of the rotor slots.

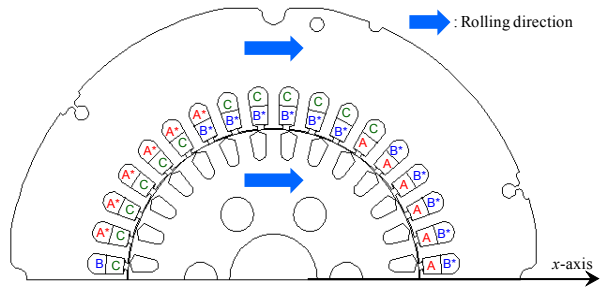

(a) two-pole three-phase induction motor

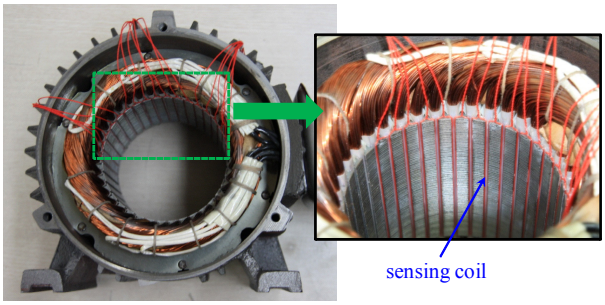

(b) stator core with sensing coils for linkage

Fig. 6 A two-pole three-phase induction motor model without rotor conducting bars.

Table 1 Specification of the induction motor model.

Item	Specification
Applied voltage	110 [V]
Frequency	60 [Hz]
Axial length	105 [mm]
Air-gap length	0.37 [mm]
Stator winding turns/slot	10 [turns]
Outer radius of stator	195 [mm]
Outer radius of rotor	106.25 [mm]
Skew of rotor	1 slot

Fig. 8 shows the B- and H-vectors calculated by the E&S vector hysteresis model. It is observed that the directions of B are not identical with those of H at whole areas, and especially there are large phase differences between B and H around region 2 with existence of the rotating magnetic field. Even in region 3 of the stator teeth having alternating magnetic fields, the phase differences occur. These phenomena cannot be observed through FEA using the scalar magnetic properties.

Fig. 9 shows the B- and H-loci obtained from the E&S vector hysteresis model, and it can be seen that the rotating magnetic fields are existed in the most parts of the stator core. In Fig. 9(b) and (c) having rotating magnetic field, it is found that the maximum magnitude of H-locus is different according to the inclination angle of

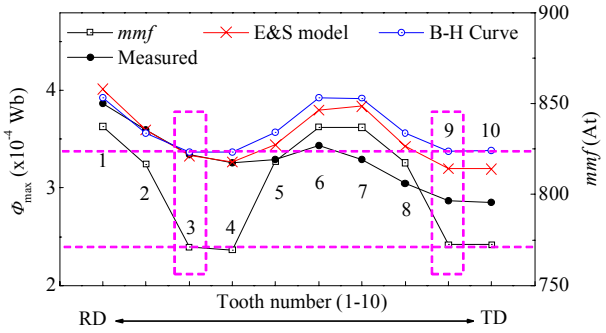

Fig. 7 Magnetic flux linkages at stator teeth where the first and tenth correspond to RD and TD, respectively.

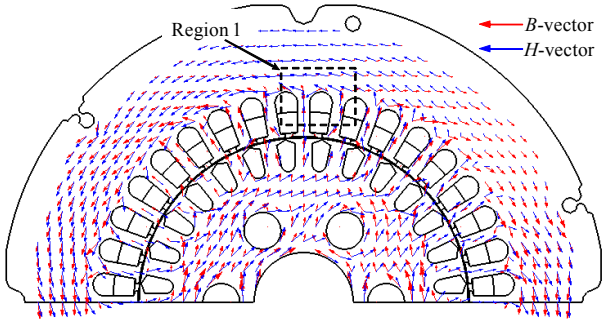

(a) whole region

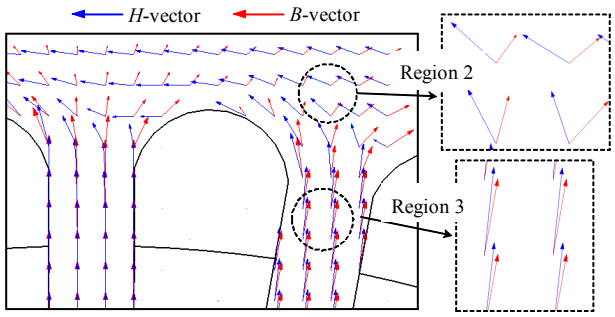

(b) region 1

Fig. 8 *B*- and *H*-vectors obtained from the E&S vector hysteresis model.

B-locus under same maximum magnitude of *B*-locus.

Fig. 10 compares the distribution of maximum magnetic flux density, maximum magnetic field intensity and iron loss, calculated from the *B*-*H* curve and E&S vector hysteresis models. In the *B*-*H* curve model, the iron loss corresponding to the maximum value of magnetic flux density, B_{max}, is obtained from the measured data under purely sinusoidal alternating *B*-waveform with frequency of 60(Hz) [8]. In the E&S vector hysteresis model, the iron loss is calculated directly from the analyzed *B*- and *H*-waveforms shown in Fig. 9 by using the following equation:

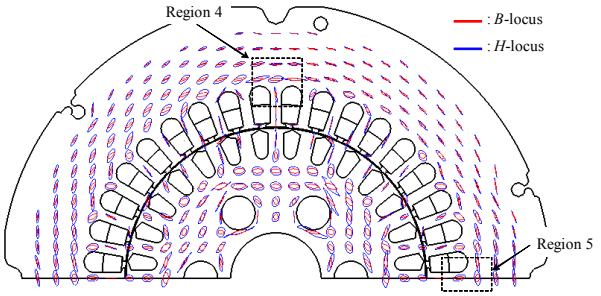

(a) whole region

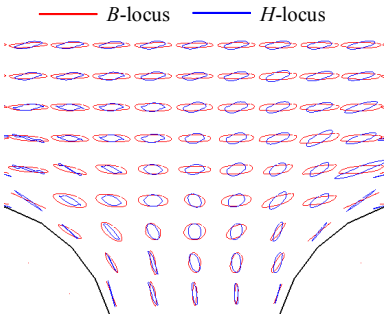

(b) region 4

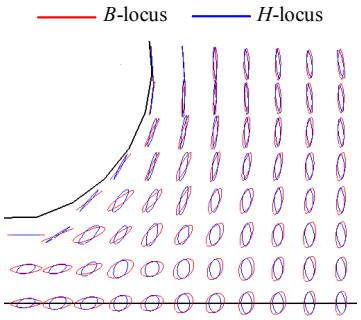

(c) region 5

Fig. 9 *B*- and *H*-loci obtained from the E&S vector hysteresis model.

$$P = \frac{1}{\rho T}\int_{o}^{T}\left(H_x\frac{dB_x}{dt} + H_y\frac{dB_y}{dt}\right)dt \quad [W/kg] \tag{3}$$

where T is the period of the exciting current and ρ is mass density of the electrical steel sheet.

It is found that the E&S vector hysteresis model gives higher magnetic flux densities and iron losses in the stator core along TD than RD. In contrast, the *B*-*H* curve model estimates same distributions of the magnetic flux density and iron loss regardless of the direction in the stator core. These asymmetric distributions by the E&S vector hysteresis model come from the anisotropic magnetic properties of the non-oriented ESS, and are verified through local distribution measurement of the magnetic flux density and iron loss in a three-phase induction motor model reported in [7].

In the numerical results calculated by the E&S vector

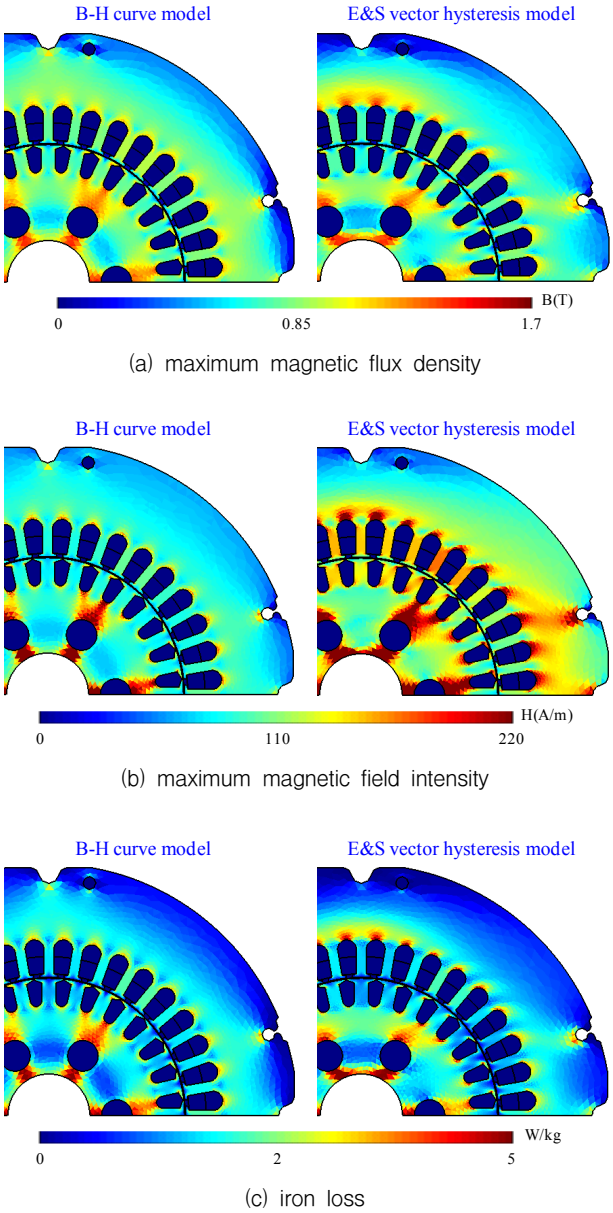

Fig. 10 Maximum magnetic flux density, maximum magnetic field intensity and iron loss distributions calculated by the *B-H* curve and the E&S vector hysteresis models.

hysteresis model, while the maximum magnetic flux densities are higher along RD than TD in the stator teeth, the corresponding maximum magnetic field intensities are higher along TD than RD due to the affect of the anisotropic magnetic property. This tendency is observed in the whole stator core, and cannot be found in the numerical results calculated by the *B-H* curve model.

4. Conclusion

In this paper, the iron loss analysis of the three-phase induction motor model considering the vector magnetic properties of the ESS is presented, and the influences of the vector magnetic properties are investigated by comparing with the numerical results from the typical *B-H* curve model.

The conspicuous features by the vector magnetic properties are summarized as follows: 1) The direction of magnetic field intensity is not parallel to that of magnetic flux density under not only the alternating but also rotating magnetic fields, 2) While the typical *B-H* curve model gives symmetric magnetic field and iron loss distributions over the whole region, the E&S vector hysteresis model does not. 3) The distributions of the magnetic field intensity and iron loss strongly depend on axis ratio and inclination angle of the magnetic flux density even in the non-oriented electrical steel sheet.

감사의 글

이 논문은 2010년도 충북대학교 학술연구지원사업의 연구비 지원에 의하여 연구되었음.

References

[1] A. J. Moses, "Importance of rotational losses in rotating machines and transformers," *Journal of Mat. Eng. and Perf.*, vol. 1, no. 2, pp. 235-244, 1992.

[2] M. Enokizono, T. Suzuki, J. Sievert, and J. Xu, "Rotational power loss of silicon steel sheet," *IEEE Trans. Magn.*, vol. 26, no. 5, pp. 2562-2564, May 2003.

[3] H. Nam, K. H. Ha, J. J Lee, J. P. Hong, and G. H. Kang, "A study on iron loss analysis method considering the harmonics of the flux density waveform using iron loss curves tested on Epstein Samples," *IEEE Trans. Magn.*, vol. 39, no. 3, pp. 1472-1472, May 2003.

[4] H. J Kim, C. S. Koh, S. K. Hong, and P. S. Shin, "Double-excitation type single sheet tester for the measurement of the magnetic characteristics of the electrical steel sheets," *Trans. of KIEE*, vol. 54-B, no. 10, pp.461-469, Oct. 2005.

[5] H. Yoon, M. Song, I. Kim, P. S. Shin, and C. S. Koh, "Accuracy improved dynamic E&S vector hysteresis model and its application to analysis of iron loss distributions in a three-phase induction motor," *IEEE Trans. Magn.*, vol. 48, no. 2, pp. 887-890, Feb. 2012.

[6] M. Song, H. Yoon, H. Yang, and C. S. Koh, "A generalized Chua-type vector hysteresis model for both the non-oriented and grain-oriented electrical steel sheets," *IEEE Trans. Magn.*, vol. 47, no. 5, pp. 1146-1149, May 2011.

[7] M. Enokizono, S. Fujiyama, H. Simoji, and J. Sievert, "Localized distribution of two-dimensional magnetic properties in three-phase induction motor core model," *J. Magn. Magn. Mater.*, vol. 215-216, pp. 772-775, Jun. 2000.
[8] [Online].Available: http://www.steel-n.com/esales/general/us/catalog/electrical/plate6.html

저 자 소 개

윤 희 성 (尹 熙 盛)

1982년 1월 17일생. 2005년 충북대학교 전기전자공학부 졸업(학사). 2005년~2007년 동 대학원 전기공학과 졸업(석사). 2007년~2012년 동 대학원 전기공학과 졸업(박사). 2012년~현재 동 대학원 박사 후 연구원.
Tel : 043-274-2426
E-mail : hsyoon@chungbuk.ac.kr

고 창 섭 (高 彰 燮)

1986년 서울대학교 전기공학과 졸업(학사). 1988년 동 대학원 전기공학과 졸업(석사). 1992년 동 대학원 전기공학과 졸업(박사). 1993~1994년 미국 Florida International University 전기컴퓨터 공학과 박사 후 연구원. 1994~1996년 삼성전기(주) 종합연구소 선임연구원. 2003년 2월~2004년 1월 미국 Texas A&M University, 전기컴퓨터공학과 객원 교수, 1996년~현재 충북대학교 전자정보대학 전기공학과 교수.
Tel : 043-261-2426
Fax : 043-274-2426
E-mail : kohcs@chungbuk.ac.kr